Yeast ORC sumoylation status fine-tunes origin licensing

Gemma Regan-Mochrie,[1,2] Timothy Hoggard,[3] Nikhil Bhagwat,[4,5] Gerard Lynch,[1] Neil Hunter,[4,5] Dirk Remus,[1] Catherine A. Fox,[3] and Xiaolan Zhao[1]

[1]Molecular Biology Program, Memorial Sloan Kettering Cancer Center, New York, New York 10065, USA; [2]Gerstner Sloan Kettering Graduate School of Biomedical Sciences, Memorial Sloan Kettering Cancer Center, New York, New York 10065, USA; [3]Department of Biomolecular Chemistry, School of Medicine and Public Health, University of Wisconsin, Madison, Wisconsin 53706, USA; [4]Howard Hughes Medical Institute, University of California at Davis, Davis, California 95616, USA; [5]Department of Microbiology and Molecular Genetics, University of California at Davis, Davis, California 95616, USA

Sumoylation is emerging as a posttranslation modification important for regulating chromosome duplication and stability. The origin recognition complex (ORC) that directs DNA replication initiation by loading the MCM replicative helicase onto origins is sumoylated in both yeast and human cells. However, the biological consequences of ORC sumoylation are unclear. Here we report the effects of hypersumoylation and hyposumoylation of yeast ORC on ORC activity and origin function using multiple approaches. ORC hypersumoylation preferentially reduced the function of a subset of early origins, while Orc2 hyposumoylation had an opposing effect. Mechanistically, ORC hypersumoylation reduced MCM loading in vitro and diminished MCM chromatin association in vivo. Either hypersumoylation or hyposumoylation of ORC resulted in genome instability and the dependence of yeast on other genome maintenance factors, providing evidence that appropriate ORC sumoylation levels are important for cell fitness. Thus, yeast ORC sumoylation status must be properly controlled to achieve optimal origin function across the genome and genome stability.

[*Keywords*: ORC; replication initiation; MCM; sumoylation; replication regulation]

Supplemental material is available for this article.

Received April 4, 2022; revised version accepted July 14, 2022.

Faithful duplication of the genome is critical for the development and health of organisms. The initiation of this process is carefully orchestrated and relies on the conserved origin recognition complex (ORC) (Bell and Stillman 1992). Composed of the Orc1–6 subunits, ORC marks replication initiation sites (origins) by binding directly to DNA and recruiting other replication initiation factors. To date, ORC is best examined in budding yeast, in which it defines ~400 specific origins in G1 phase and collaborates with the Cdc6 protein to recruit and load the MCM replicative helicase complex onto origin DNA, a process referred to as origin licensing (Bell and Labib 2016). In the subsequent S phase, origins are activated by several replication initiation factors, including the DDK kinase, so that MCM can direct replisome assembly and unwind the parental DNA duplex to permit nascent strand synthesis (Bell and Labib 2016).

The global regulation of origin function affects genome stability and cell fate determination and thus is a vital aspect of genome maintenance (Smith et al. 2001; Watanabe and Maekawa 2010; Ryba et al. 2011; Debatisse et al. 2012; Pozo et al. 2018). The use or firing of individual origins is affected by both origin licensing and origin activation, and each of these distinct steps can be controlled at multiple levels. Budding yeast offers a valuable system for examining the complexities of the regulation of origin function because its origins are mapped, and genetic, genomic, and biochemical tools are available to probe both positive and negative modes of regulation (Bell and Labib 2016). Examples of positive origin regulators uncovered in yeast thus far include the Fkh1 and Fkh2 proteins that bind adjacent to a subset of origins to promote ORC–origin binding and consequently origin licensing, as well as DDK recruitment to origins and consequently origin activation (Lei et al. 1997; Knott et al. 2012; Fang et al. 2017; Hoggard et al. 2020). Countering positive regulation, the Sir2 and Sir3 proteins promote repressive chromatin at a subset of origins to reduce their licensing probability (Hiraga et al. 2014; Hoggard et al. 2018, 2020). In addition, replication initiation factors such as DDK and the MCM cofactor Cdc45 are limiting in cells; thus, their affinity for specific origins positively correlates with origin firing

Corresponding author: zhaox1@mskcc.org
Article published online ahead of print. Article and publication date are online at http://www.genesdev.org/cgi/doi/10.1101/gad.349610.122.

timing and overall origin function (Mantiero et al. 2011; Tanaka et al. 2011; Saner et al. 2013; Tanaka and Araki 2013). Generally, origins that fire in early S phase (early origins) tend to be more effective at competing for the limiting origin activation factors (Mantiero et al. 2011; Tanaka et al. 2011). As such, altering early origin firing can indirectly alter the use of origins that fire later in S phase (Knott et al. 2012; Hoggard et al. 2020). Collectively, studies thus far have revealed multilayered regulation of origin function at the level of both licensing and activation; however, a full picture has yet to be achieved.

Multiple origin-binding factors are sumoylated in both yeast and humans, suggesting that this protein modification is relevant to the regulation of origin function (Golebiowski et al. 2009; Cremona et al. 2012). Sumoylation is a highly dynamic protein modification that targets a large array of proteins and influences substrate functions by diverse mechanisms (Zhao 2018). Understanding the roles of sumoylation on any substrate requires establishing approaches where its sumoylation status can be specifically altered. Here we focus on the ORC complex that is sumoylated in both yeast and human cells, as revealed by proteomic screens under stress conditions (Golebiowski et al. 2009; Cremona et al. 2012). Currently, the biological consequences of ORC sumoylation are poorly understood.

To address the above question, we established that multiple yeast ORC subunits are sumoylated during unperturbed growth, indicating that this modification is not confined to stress conditions. We then generated both hypersumoylated and hyposumoylated ORC and examined the consequences to ORC function in chromosome replication. Genome-scale assessment of origin firing in an ORC hypersumoylation situation revealed selective repression of origin function, particularly that of early origins, and reduced chromatin-associated MCM during G1 phase. Consistent with these in vivo data, MCM loading reactions performed with reconstituted proteins revealed that sumoylated ORC inhibited MCM recruitment to origin DNA. Furthermore, determination of a specific endogenous sumoylation site on Orc2 using mass spectrometry allowed the generation of a single-residue substitution mutant that led to reduced Orc2 sumoylation. This hyposumoylated ORC mutant had an origin firing phenotype opposite to that caused by hypersumoylated ORC; namely, enhanced firing of a subset of early origins. Finally, although hypersumoylated and hyposumoylated ORC showed opposing effects on origin function, both resulted in genomic instability and required other genome stability factors for optimal growth. These data provide evidence that appropriate ORC sumoylation levels are required to promote the normal spatiotemporal dynamics of origin function that in turn are important for genome stability.

Results

Multiple ORC subunits were sumoylated during normal growth

Our previous work identified ORC sumoylation under DNA damage conditions in yeast (Cremona et al. 2012). Here we tested whether ORC subunits were sumoylated during normal growth. We used an established method for sumoylation detection, in which sumoylated proteins are enriched on Ni-NTA resin due to binding of endogenously expressed 8His-tagged yeast SUMO (Smt3), referred to as nickel pull-down (Ni-PD) (Ulrich and Davies 2009). The procedure was carried out under denaturing conditions to limit desumoylation during extraction and contamination of other proteins through protein–protein interactions. Each endogenous ORC subunit was tagged at its C terminus with a 6HA epitope that is lysine-free to avoid potential sumoylation of the tag itself. Viable cells were obtained for four out of the six ORC subunits. While HA-tagged Orc2, Orc4, and Orc5 supported normal growth, similarly tagged Orc1 showed slower growth (Supplemental Fig. S1A). The sumoylation levels in all four HA-tagged strains were examined.

For each ORC subunit examined, Ni-PD eluate was evaluated by immunoblotting using an anti-HA antibody. Unmodified forms of HA-tagged ORC subunits that migrated at their expected molecular weight were detected at low levels due to nonspecific histidine-mediated binding to Ni-NTA resin, as previously documented for other proteins (Fig. 1A, orange circles; Cremona et al. 2012; Wei and Zhao 2016; Dhingra et al. 2019). Importantly, modified forms unique to each ORC protein were detected as slower migrating bands (Fig. 1A, teal triangle). These modified forms exhibited the typical reduced migration in SDS-PAGE caused by sumoylation, as a single SUMO moiety causes an ~20-kDa protein band upshift (Ulrich and Davies 2009). These sumoylated forms were further verified, as they were only detected in the presence of 8His-SUMO, but not with untagged SUMO, whereas unmodified forms were detected in both conditions (Supplemental Fig. S1B).

We observed that sumoylation levels for Orc1, Orc2, and Orc4 were higher than for Orc5 (Fig. 1A). In addition, monosumoylated and multisumoylated or polysumoylated forms were seen for Orc1, Orc2, and Orc4, while Orc5 mainly exhibited a monosumoylated form (Fig. 1A). Two distinct monosumoylated Orc4 forms were observed, likely due to two different sites of monosumoylation, leading to different migration rates, as seen for other sumoylated targets such as PCNA or Rfa1 (Fig. 1A; Papouli et al. 2005; Dhingra et al. 2019). Taken together, these data provided evidence that multiple ORC subunits were sumoylated during normal cell growth, and that each sumoylated ORC subunit had a distinct sumoylation status.

ORC2-SuON *caused ORC hypersumoylation and cell lethality*

Next, we assessed the consequences of altering ORC sumoylation levels. First, we generated an ORC hypersumoylation construct. The strategy used exploits a high-affinity SUMO interaction domain to promote sumoylation of its fusion partner and possibly closely associated subunits, presumably by increasing local SUMO concentrations (Almedawar et al. 2012). This tag, referred to as SuON, has been used to efficiently enhance the sumoylation of several proteins (Almedawar et al. 2012; Bonner

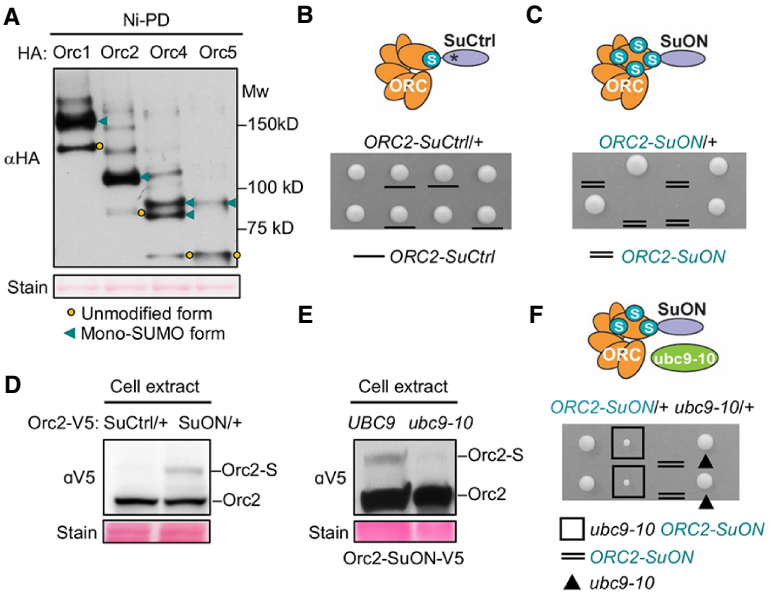

Figure 1. Increasing ORC sumoylation led to cell lethality that could be rescued by a SUMO E2 mutant. (*A*) Sumoylation of Orc1, Orc2, Orc4, and Orc5 was detected under normal growth conditions. Sumoylated forms of each HA-tagged protein were enriched by Ni-PD. Unmodified and sumoylated bands are indicated by orange circles and filled teal arrows, respectively. Equal loading is indicated by Ponceau stain (Stain). (*B*) The SuCtrl tag fused with Orc2 supported normal growth. (*Top*) A cartoon depicting the fusion of the SuCtrl to the Orc2 subunit of the ORC complex. (S) SUMO. The asterisk indicates a point mutation in the SUMO binding domain (see the text). (*Bottom*) Representative tetrads from a diploid strain heterozygous for *ORC2-SuCtrl*. Cells were grown for 2 d at 30°C. Strains were also heterozygous *8His-SMT3*, which did not affect growth. (*C*) Orc2 fused with SuON caused cell lethality. (*Top*) A cartoon depicting the SuON tag fusion to the Orc2 subunit to increase ORC sumoylation. Symbols are as in *B*. (*Bottom*) Representative tetrads are shown as in *B*. (*D*) *ORC2-SuON* led to increased Orc2 sumoylation. Whole-cell extracts were examined by immunoblotting; the unmodified and sumoylated forms are indicated. Equal loading is indicated by the Ponceau stain. (*E*) *ubc9-10* reduced Orc2 sumoylation caused by *ORC2-SuON*. Orc2 sumoylation levels were examined in cells containing a single copy of wild-type or mutant *UBC9*. (*F*) Cell lethality caused by *ORC2-SuON* was rescued by *ubc9-10*. (*Top*) A cartoon depicting that, in principle, *ubc9-10* could reduce ORC sumoylation. (*Bottom*) Representative tetrads are shown as in *B* except that cells were grown for 3 d at 24°C.

et al. 2016; Wei and Zhao 2016). The same tag containing a single point mutation at the key SUMO binding residue was used as a control and is referred to as SuCtrl (Almedawar et al. 2012).

We chose to tag Orc2, as it tolerated C-terminal tags well (Supplemental Fig. S1A) and its sumoylation forms were easily detectable (Fig. 1A). The SuON or SuCtrl tag sequence was inserted at the 3′ end of one copy of the *ORC2* gene in diploid cells, followed by sporulation to produce untagged and tagged versions of *ORC2*. *ORC2-SuCtrl* fusion supported wild-type growth, suggesting the tag was tolerated by Orc2 (Fig 1B, bottom panels). In contrast, *ORC2-SuON* fusion-containing cells were not recovered (Fig 1C, bottom panel), providing evidence that hypersumoylation of ORC caused cell lethality.

Given that SuON does not cause cell lethality when fused to other proteins, despite increasing sumoylation of its fusion partners (Almedawar et al. 2012; Bonner et al. 2016; Wei and Zhao 2016), we reasoned that the *ORC2-SuON* lethality was due to hypersumoylation of Orc2 and/or other ORC subunits. Indeed, examination of protein extracts showed higher Orc2 sumoylation levels in diploid cells containing *ORC2-SuON* compared with *ORC2-SuCtrl* (Fig. 1D). Global sumoylation levels were similar between these diploid cells, suggesting the specificity of *ORC2-SuON* (Supplemental Fig. S1C). Thus *ORC2-SuON* cell inviability was most likely caused by excessive ORC sumoylation.

Lethality caused by ORC hypersumoylation was rescued by reducing SUMO E2 function

To further test the notion that *ORC2-SuON* cell lethality was due to increased ORC sumoylation, we repeated the SuON tagging of Orc2 in diploid cells heterozygous for a mutant allele of the SUMO E2 enzyme Ubc9 (*ubc9-10*) (Cremona et al. 2012; Lei and Zhao 2017). If excessive ORC sumoylation were causing lethality, then the *ubc9-10* mutant would be predicted to reduce ORC sumoylation and rescue the cell lethality caused by *ORC2-SuON*. While Ubc9 is essential, *ubc9-10* supports normal growth at its permissive temperature of 24°C, with moderately reduced levels of global sumoylation (Cremona et al. 2012; Lei and Zhao 2017).

At 24°C, *ubc9-10* cells exhibited reduced Orc2 sumoylation levels in cells containing *ORC2-SuON* (Fig. 1E). Furthermore, haploid spore clones containing both *ORC2-SuON* and *ubc9-10* were viable, albeit slow growing, in contrast to the inviable *ORC2-SuON* spore clones (Fig. 1F). These data provided additional evidence that the inviability of *ORC2-SuON* cells was due to increased sumoylation of ORC.

As *ubc9-10* allows for *ORC2-SuON* cell viability, haploid cells that contain either *ORC2-SuON* or *ORC2-SuCtrl* as the only copy of *ORC2* could be compared in a *ubc9-10* background. *ORC2-SuON* led to a higher level of sumoylated Orc2 even in a *ubc9-10* background as compared with *ORC2-SuCtrl* (Supplemental Fig. S1D). Thus, this system allowed us to further examine the effects of ORC hypersumoylation. Because the SuON tag can increase the sumoylation of other subunits within a complex when fused to a single subunit (Almedawar et al. 2012; Bonner et al. 2016; Wei and Zhao 2016), we examined sumoylation of Orc1 and Orc4 in *ORC2-SuON ubc9-10* cells. *ORC2-SuON* enhanced Orc1 and Orc4 sumoylation compared with the *ORC2-SuCtrl* cells (Supplemental Fig. S1E,F). Thus, the *Orc2-SuON* fusion caused hypersumoylation of multiple ORC subunits.

However, Orc2-SuON and Orc2-SuCtrl cells showed similar levels of sumoylation of the Mcm2 and Mcm3 subunits of the replicative helicase that binds to ORC at origins during origin licensing (Supplemental Fig. S1G). Thus, Orc2-SuON likely limited hypersumoylation only to ORC itself.

ORC hypersumoylation reduced the firing of a subset of origins

We exploited the viability of *ORC2-SuON ubc9-10* cells to examine the consequences of excessive ORC sumoylation on origin function. Specifically, whole-genome sequencing of G1-phase and S-phase cells was used to generate high-resolution replication profiles for both *ORC2-SuON ubc9-10* and congenic *ORC2-SuCtrl ubc9-10* cells. In these experiments, DNA copy number changes (S/G1 ratios) were used to derive replication profiles for each chromosome (Hawkins et al. 2013). As shown in the example of chromosome VII, compared with *ORC2-SuCtrl* cells, cells containing *ORC2-SuON* exhibited an alteration of S-phase copy number at some origins (Fig. 2A; Supplemental Fig. S2). These data provided evidence that the function of specific origins was sensitive to ORC hypersumoylation.

Next, a quantitative approach was used to identify the groups of origins affected by Orc2-SuON. To this end, each origin was assigned a *Z*-score represented by its S to G1 ratio of sequenced reads to reflect its replication behavior (Hoggard et al. 2021). A kernel density estimation was performed to generate a graph of origin density (*Y*-axis) versus *Z*-scores (*X*-axis) (Fig. 2B). This graph revealed the genome-scale effects of ORC hypersumoylation on origin firing. The *ORC2-SuCtrl* data generated a plot with a shoulder and two clearly distinguished peaks, corresponding to the known "early," "mid," and "late" origin waves of replication (Fig. 2B, gray trace). In contrast, the *ORC2-SuON* profile generated only a single peak centered between the mid-S and late-S origins (Fig. 2B, teal trace). Thus, ORC hypersumoylation altered the normal pattern of temporal control of origin firing, with origins normally activated in distinct halves of S phase (first half, early; second half, and late) acting more similarly.

The graph in Figure 2B provides evidence that the replication of a significant number of early origins was relatively delayed and/or that replication of a significant number of late origins was accelerated. To test this notion further, the *Z*-score ratio of *ORC2-SuON*/*ORC2-SuCtrl* was determined for each origin. A negative ratio (cutoff of <0.8) indicated that an origin's firing was relatively reduced in *ORC2-SuON* cells, whereas a positive value (cutoff of >1.2) suggested the opposite. By these criteria, the firing of 35 origins was reduced (negative) and the firing of 43 origins was enhanced (positive) by ORC hypersumoylation (Fig. 2C). These origins were further parsed by their experimentally determined replication times, and the data are displayed in stacked histograms (Fig. 2C; Yabuki et al. 2002). These analyses revealed that among the affected origins, ORC hypersumoylation preferentially reduced the firing of early origins relative to mid- and late-acting origins and, conversely, enhanced that of late origins. This conclusion was consistent with the current model that reducing the ability of early origins to compete for limited replication factors enhances the availability of such factors to late origins. Thus, we posit that ORC hypersumoylation directly reduced the firing of a subset of early origins, likely via dampening origin licensing, and in doing so, allowed for a relative increase in the firing of some late origins.

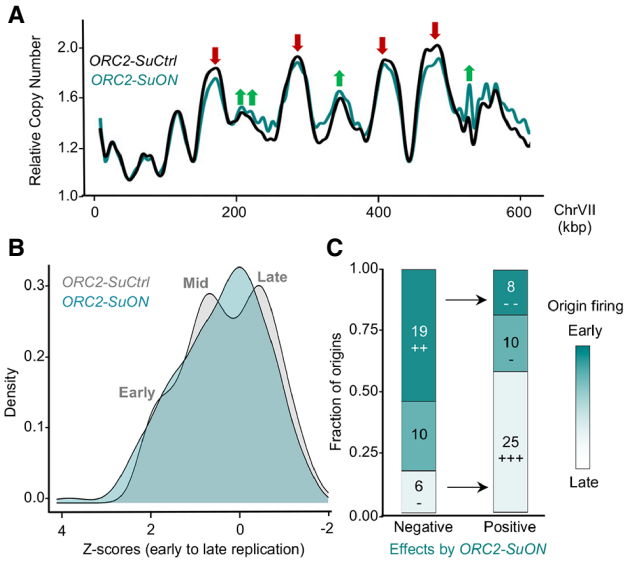

Figure 2. *ORC2-SuON* led to preferential inhibition of a subset of early origins and a temporally homogenized replication profile. (*A*) Copy number analysis based on genome sequencing data depicted as a chromosomal replication scan for chromosome VII for *ORC2-SuCtrl* (black) and *ORC2-SuON* (teal) cells. Red and green arrows mark the origins that show decreased and increased firing in *ORC2-SuON* compared with *ORC2-SuCtrl* cells, respectively. (*B*) *ORC2-SuON* altered the replication timing program. Kernel density estimation was used to generate a plot of origin *Z*-scores versus density of replication origins in *ORC2-SuON* (teal) and *ORC2-SuCtrl* (gray). (*C*) The *ORC2-SuON*/*ORC2-SuCtrl* *Z*-score ratio was determined for each origin, and the origins negatively affected (ratio cutoff of <0.8) or positively affected (ration cutoff of >1.2) by *ORC2-SuON* were parsed by their experimentally determined Trep value (Yabuki et al. 2002). The *P*-values for enrichment (+) or depletion (−) of the various types of Trep origins among affected origins are indicated. (+++/− − −) $P \leq 0.001$, (++/− −) $P \leq 0.01$, (+/−) $P \leq 0.05$.

ORC hypersumoylation reduced MCM recruitment to origin DNA

ORC's established biochemical role at replication origins is to recruit and load the MCM complex in the origin licensing process, and therefore reduced MCM loading onto chromosomal DNA is a likely mechanism by which *ORC2-SuON* reduced origin function. To test this idea, the effects of ORC sumoylation were examined in a reconstituted MCM recruitment and loading system (Remus et al. 2009). In this system, purified yeast ORC was first loaded onto origin-containing DNA immobilized on

paramagnetic beads (Fig. 3A, step 1). Then, one-half of the DNA-bound ORC was subjected to a reconstituted sumoylation reaction, which used purified sumoylation machinery and ATP (Zhao and Blobel 2005), while the other half served as the control reaction by omitting SUMO (Fig. 3A, step 2). Robust ORC sumoylation was achieved only in the reactions that included SUMO, and sumoylation did not reduce ORC retention on DNA beads (Fig. 3B; Supplemental Fig. S3A, lanes 2,6). We note that ORC subunits were sumoylated to varying degrees similar to observations in vivo under the conditions used here. The analyses indicate that Orc1–3 were abundantly sumoylated because only slower migrating sumoylated forms were detected, while Orc4–6 were sumoylated to a lesser degree because unmodified forms of these subunits were easily detected (Supplemental Fig. S3B).

The sumoylation machinery and ATP in both the reaction and the control were removed from the DNA beads (Fig. 3A, step 3). This step was followed by the addition of purified Cdc6 and MCM-Cdt1 in the presence of either ATPγS or ATP to initiate MCM recruitment or to allow for a complete loading reaction, respectively (Fig. 3A, step 4). ATP hydrolysis-dependent MCM loading resulted in the formation of a MCM double hexamer topologically bound to the DNA that was resistant to high-salt wash, whereas MCM that was only recruited to ORC–Cdc6–DNA but not loaded, as occurs in the presence of ATPγS, was washed off with high-salt buffer (Fig. 3A, step 5; Remus et al. 2009; Sun et al. 2013). As such, this experimental setup can assess both "MCM loading" and "MCM recruitment" (Fig. 3A, step 6).

In the presence of ATPγS and a low-salt wash, "MCM recruitment" was efficient in the absence of ORC sumoylation, as seen previously (Fig. 3B; Supplemental Fig. S3A, lane 1). However, MCM recruitment was greatly reduced upon ORC sumoylation (Fig. 3B; Supplemental Fig. S3A, lane 2). As expected, no MCM was recovered on DNA in the presence of ATPγS after a high-salt wash regardless of ORC sumoylation (Fig. 3B; Supplemental Fig. S3A, lanes 3,4). In the presence of ATP and a high-salt wash, MCM loading was observed in the absence, but not the presence, of ORC sumoylation (Fig. 3B; Supplemental Fig. S3A, lanes 7,8). Importantly, defective MCM recruitment associated with ORC sumoylation was reversed by removing sumoylation using the purified desumoylation enzyme Ulp1 prior to the addition of MCM (Fig. 3C; Supplemental Fig. S3C). Thus, the ORC–DNA complex was fully capable of recruiting and loading MCM once sumoylation was removed. Therefore, ORC hypersumoylation directly inhibited MCM loading in vitro by impeding MCM recruitment to the ORC–origin DNA complex.

To test whether ORC sumoylation also reduced MCM association with chromatin in vivo, yeast cells arrested in G1 were examined for chromatin-bound MCM levels using a standard chromatin fractionation assay (Schepers and Diffley 2001). The Mcm2 signal from the chromatin fraction in *ORC2-SuON* cells was reduced approximately twofold compared with *ORC2-SuCtrl* cells, while the level in the supernatant was concomitantly increased (Fig. 3D). Taken together, the in vivo and in vitro data provided evidence that ORC hypersumoylation inhibits MCM recruitment to origins. Accordingly, the alterations in replication origin firing observed in *ORC2-SuON* cells could be explained by reduced origin licensing efficiency.

ORC hypersumoylation compromised rDNA replication and stability

Thus far, we have focused on nonrepetitive regions of the genome. It is established that replication and stability of

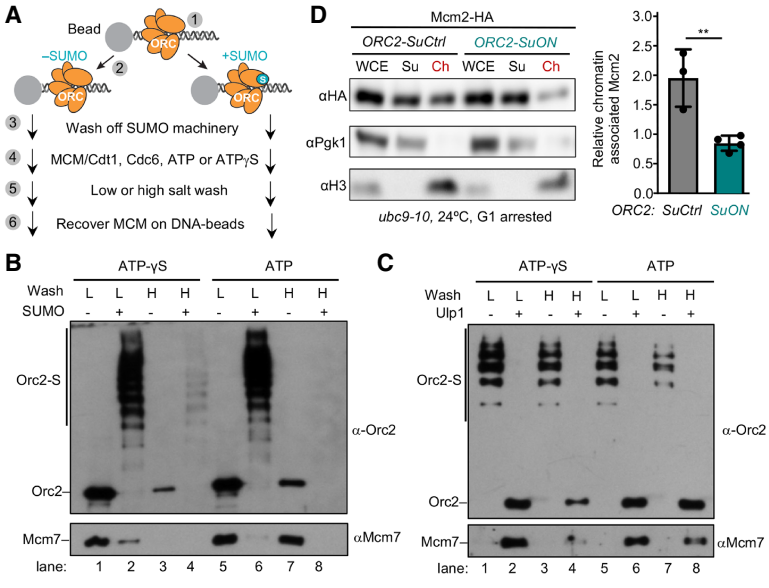

Figure 3. ORC hypersumoylation prevented MCM loading. (*A*) Reaction scheme to determine the impact of ORC hypersumoylation on MCM recruitment and loading in vitro (see the text for details). (*B*) Immunoblot analysis of DNA-bound fractions to assess Orc2 and Mcm7 DNA association in vitro. Following ORC sumoylation (+) or mock treatment (–), MCM loading reactions were performed in the presence of ATPγS (lanes *1–4*) or ATP (lanes *5–8*), as indicated. DNA beads were washed with low-salt (L) or high-salt (H) buffer, as indicated. (*C*) Immunoblot analysis of Orc2 and Mcm7 association with DNA in vitro. Following ORC sumoylation, MCM loading reactions were performed in the absence (–) or presence (+) of Ulp1 and either ATPγS (lanes *1–4*) or ATP (lanes *5–8*). DNA beads were washed with either low-salt (L) or high-salt (H) buffer. (*D*) Assessment of chromatin-bound and soluble MCM from G1-arrested *ORC2-SuCtrl* and *ORC2-SuON* cells. (*Left*) Immunoblot showing Mcm2 in the soluble and chromatin fractions in G1 cells. Pgk1 served as the soluble control, while histone H3 served as the chromatin-bound control. (*Right*) Quantification of the ratio of Mcm2 to H3 recovered in the chromatin fraction. An unpaired two-tailed *t*-test generated a *P*-value of <0.01 (**) for the difference between Mcm2 recovery in *ORC2-SuCtrl* and in *ORC2-SuON* cells.

the repetitive ribosomal DNA (rDNA) is particularly sensitive to defects in replication initiation factors, including ORC mutants (Kwan et al. 2013; Salim et al. 2017; Sanchez et al. 2017). We therefore examined whether *ORC2-SuON* compromised the replication and stability of the rDNA. First, pulsed-field gel electrophoresis (PFGE) was used to examine chromosomal replication efficiency. In this assay, only fully replicated chromosomes can enter the gel. While replication completion of all chromosomes was compromised by *ORC2-SuON*, chromosome XII, which contains the rDNA repeats, showed the most striking defects (Fig. 4A). Quantitative comparison of gel entry between the two longest chromosomes in yeast, chromosomes IV and XII, confirmed that the *ORC2-SuON*-associated replication defects were more severe for chromosome XII (Fig. 4B). Second, we used a rDNA marker loss assay to assess rDNA stability (Fig. 4C). *ORC2-SuON* increased rDNA marker loss by approximately fourfold compared with *ORC2-SuCtrl* (Fig. 4B). Together, these data provided evidence that ORC hypersumoylation caused defects in rDNA replication and stability.

Identification of the major sumoylation site on Orc2

Our examination of *ORC2-SuON* cells provided evidence that ORC hypersumoylation reduced the function of a subset of origins. To complement this analysis, a mutation in ORC that reduced ORC sumoylation was required. To this end, an endogenous sumoylation site on at least one ORC subunit first had to be identified. As biochemical mapping of sumoylation sites of endogenously expressed proteins is challenging due to the low level of sumoylated forms, we concentrated on mapping the sumoylation site(s) on the Orc2 subunit due to its relatively high level of sumoylation. Using a two-step protocol to enrich endogenously sumoylated Orc2 forms, four Orc2 sumoylation sites were identified by mass spectrometry (Fig. 5A; Supplemental Fig. S4). Three of the sites—K406, K434, and K419—were within the conserved AAA$^+$-like domain of Orc2, while the fourth site, K592, was within the Orc2 winged helix domain (WHD) (Fig. 5B).

To assess which of these four sites were most relevant for Orc2 sumoylation, gene replacement was used to convert each lysine codon to an arginine codon, alone or in combination, at the endogenous Orc2 locus. Substitution of all four lysine residues with arginine reduced Orc2 sumoylation substantially (Fig. 5C, lane 4). Notably, the single K406R substitution caused a similar reduction in sumoylation (Fig. 5C, lane 5), whereas K592R alone or the combination of K419R and K434R mildly reduced Orc2 sumoylation (Fig. 5C, lanes 1,2). Therefore, K406 was the primary site responsible for Orc2 sumoylation in vivo. Importantly, *orc2-K406R* had no effect on Orc2 protein levels or Orc2 stability on chromatin, consistent with the in vitro data showing that ORC–DNA stability was unaffected by ORC sumoylation (Fig. 5D,E). Thus, the *orc2-K406R* mutant protein reduced Orc2 sumoylation substantially but retained the most fundamental activity of ORC, binding to chromosomal DNA.

Orc2 hyposumoylation enhanced early origin firing

To assess the effects of the Orc2 sumoylation mutant on DNA replication, cell cycle progression upon release from G1 arrest was measured by FACS analyses. Compared with Orc2-6HA, the mutant *orc2-K406R-6HA* cells exhibited a two-mode alteration in S-phase progression (Fig. 6A). At early time points (25 and 30 min), more *orc2-K406R* cells were in S phase compared with *ORC2* WT cells, while at 50 and 60 min, when most *ORC2* wild-type cells had reached the 2C peak, a substantial fraction of *orc2-K406R* cells had not yet reached that point (Fig. 6A). These data provided evidence that Orc2 hyposumoylation caused DNA replication defects.

To compare the consequences of hyposumoylation versus hypersumoylation of ORC on origin function, high-resolution replication profiles as described for *ORC2-SuON* above were generated for *ORC2-6HA* and *orc2-K406R-6HA*. As exemplified by the replication profile scan of chromosome VII, *orc2-K406R* altered the firing of subsets of origins relative to *ORC2* (Fig. 6B; Supplemental Fig. S5). *Z*-score analyses for origins with

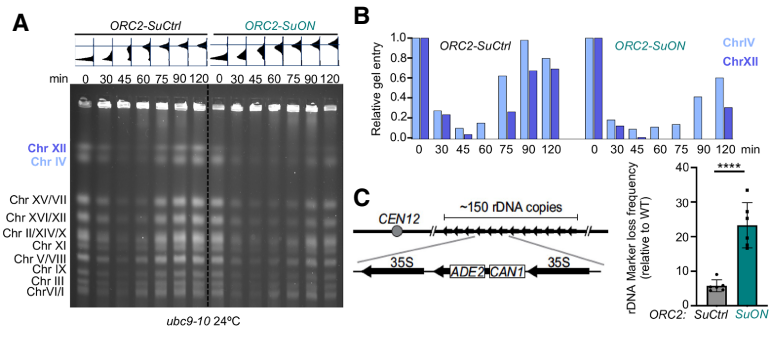

Figure 4. *ORC2-SuON* resulted in inhibition of chromosomal replication, with the most severe effects on the rDNA-containing chromosome. (*A*) PFGE analysis of *ORC2-SuCtrl* and *ORC2-SuON* cells during an S-phase time course initiated after release of cells from G1 arrest. Chromosomal DNA was stained with ethidium bromide after PFGE. The dotted line demarks the two different strains that were analyzed on the same gel. The cell cycle progress for each time point analyzed was determined by FACS and is shown *above* the gel. (*B*) DNA gel entry signal normalized to G1 for chromosome IV and chromosome XII. (*C*) The effect of *ORC2-SuON* on rDNA marker loss was determined. (*Left*) Schematic of the rDNA marker loss frequency assay. (*Right*) rDNA marker loss frequency between *ORC2-SuCtrl* and *ORC2-SuON* cells. An unpaired two-tailed *t*-test was used to generate a *P*-value of <0.0001 (****) for the difference between two types of cells.

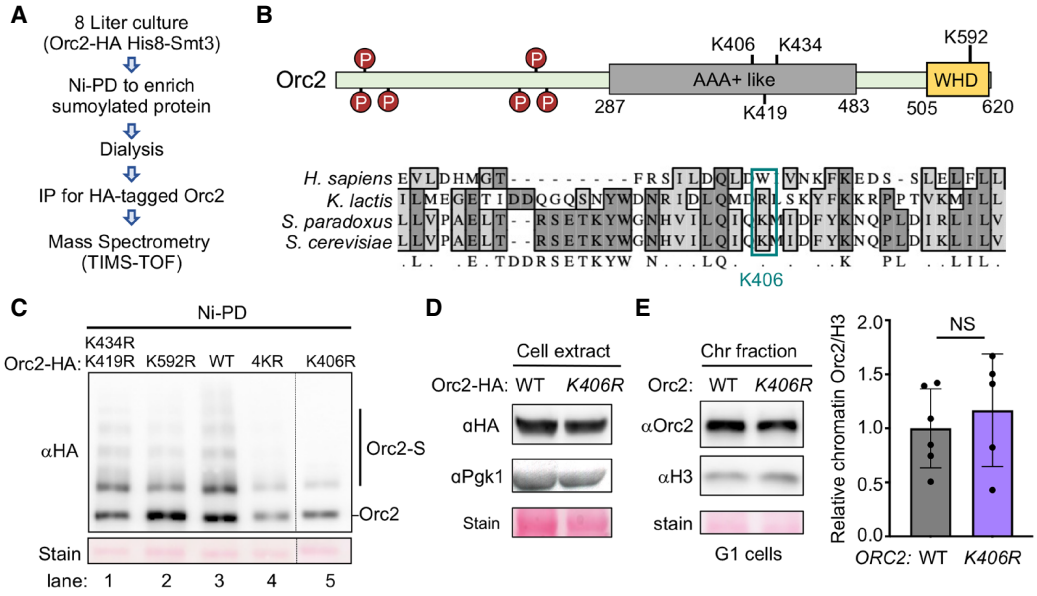

Figure 5. Mapping the Orc2 sumoylation sites. (*A*) Experimental outline for mapping endogenous Orc2 sumoylation site(s) (details are in the Materials and Methods). (*B*) Schematics of Orc2 domains and modification sites. (*Top*) CDK phosphorylation sites (P) and four lysine residues mapped via mass spectrometry. (*Bottom*) Conservation analyses of Orc2 orthologs. K406 is only conserved within the *Saccharomyces* genus. (*C*) The effects of mutating four lysine residues on Orc2 sumoylation. Orc2 sumoylation levels were compared among congenic cells that differed by the indicated *ORC2* genotypes on the same gel, with the dotted line indicating the removal of superfluous lanes. Equal loading is indicated by Ponceau-S stain (Stain). (*D*) Levels of Orc2 determined in whole-cell extracts from cells with the indicated genotypes. Pgk1 served as a loading control. The Ponceau-S-stained portion of the blot is also shown. (*E*) Orc2 in the chromatin fractionation was examined for the indicated genotype. Immunoblot results and a Ponceau-S-stained section of the membrane are at the *left*, and quantification of independent experiments are at the *right*. Two-tailed *t*-tests generated *P*-values indicating no difference in Orc2 chromatin association between the two examined genotypes.

different replication times revealed enhancement of early origin firing by *orc2-K406R* (Fig. 6C). This phenotype was generally opposite to that observed for *ORC2-SuON* as described above. To further challenge this idea on a genome scale, a kernel density estimation was performed to generate graphs of the origin density (*Y*-axis) versus the $\log_2$ of *Z*-score ratios (*X*-axis) for each *ORC2-SuON*/*ORC2-SuCtrl* (Fig. 6D, teal) and *orc2-K406R*/*ORC2* (Fig. 6D, purple) data sets (Fig. 6D). This approach provided a direct comparison of the genome-scale origin firing of hypersumoylation versus hyposumoylation of ORC, which showed the two had opposing effects on a significant number of origins (Fig. 6D). Finally, as for *ORC2-SuON*/*ORC2-SuCtrl* analyses in Figure 2C, *orc2-K406R*/*ORC2* *Z*-score ratios were determined for each origin, affected origins were divided into negatively or positively affected categories, and the origins were parsed again by their experimentally determined replication times (Fig. 6E). These analyses revealed that among affected origins, ORC hyposumoylation caused by *orc2-K406R* preferentially enhanced the firing of early origins and reduced that of late origins, showing generally the opposite consequences on affected origins compared with ORC hypersumoylation (Fig. 2C). Consistent with the dual shifts of origin function observed in *orc2-K406R-6HA* cells, gross assessment of MCM chromosomal association did not reveal a clear difference when compared with ORC2-6HA cells (Supplemental Fig. S6A).

In summary, ORC hyposumoylation caused by *orc2-K406R* enhanced the function of a subset of early origins while reducing that of a subset of late origins, the latter outcome likely being an indirect consequence of enhanced early origin function. Thus, ORC hypersumoylation and hyposumoylation had opposing effects on origin function, consistent with a negative role for ORC sumoylation on origin licensing of some early S-phase origins.

ORC hyposumoylation or hypersumoylation generated a dependence on other genome factors

Our analyses revealed that *ORC2-SuON* and *orc2-K406R* had generally opposing effects on origin firing, yet both types of effects might be expected to cause chromosomal replication imbalances that compromise genome stability and cell fitness. To test this prediction, genetic interactions of the two different ORC alleles were assessed against other relevant genome factors. First, both *ORC2-SuON* and *orc2-K406R*, but not their corresponding controls, showed negative interactions with the null allele affecting the DNA damage checkpoint protein Rad9 (Fig. 7A,B; Supplemental Fig. S6B). These data provided genetic evidence that alterations in ORC sumoylation status

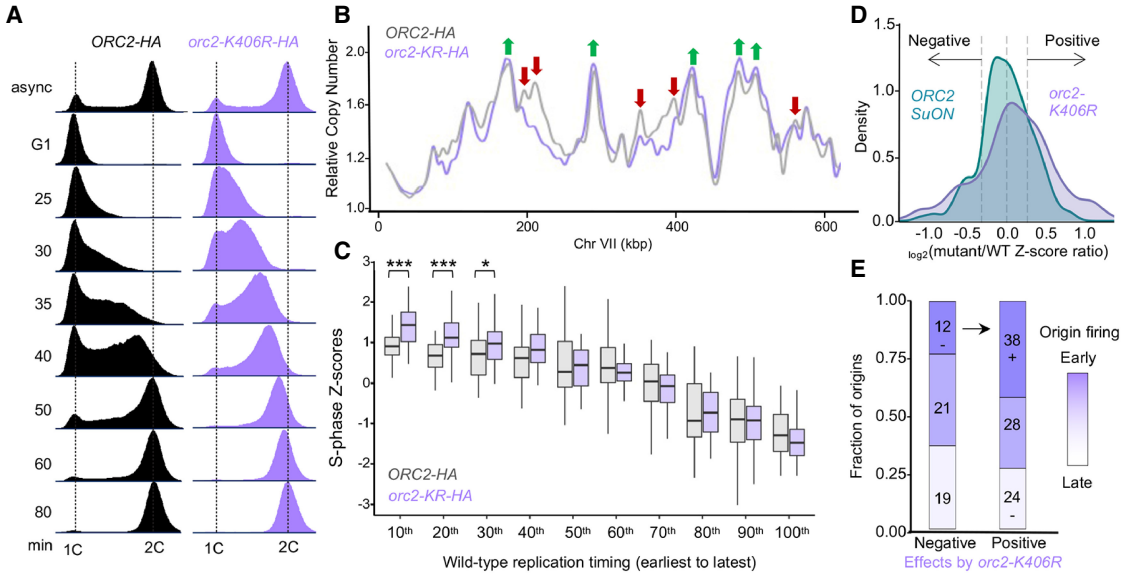

Figure 6. Orc2 hyposumoylation increased early origin firing. (*A*) *orc2-K406R* cells exhibited a biphasic replication profile, as shown by flow cytometry analysis at 24°C. At 25 and 30 min, *orc2-K406R* entered S phase more rapidly, whereas at 50 and 60 min, *orc2-K406R* appeared to be lagging behind wild-type cells. (*B*) Copy number analysis based on genome sequencing data depicted as a chromosomal replication scan for chromosome VII for *ORC2-HA* (black) and *orc2-K406-HA* (light purple) cells. Red and green arrows mark the origins that show decreased and increased firing in *orc2-K406* compared with *ORC2* cells, respectively. (*C*) *Z*-score distribution analyses. *Z*-scores were plotted for the earliest to the latest fired origins in wild-type cells. Origins were parsed into 10 distinct cohorts by their firing time. The *Z*-scores for origins within each decile are presented as box and whiskers plots from the earliest 10% (10th) to the latest 10% (100th) decile. Wilcoxon rank sum *P*-values for the differences between the two genotypes are indicated. (*) $P < 0.01$, (***) $P < 0.001$). (*D*) To compare the effects of hypermorphic Orc2 sumoylation (*ORC2-SuOn*, green) with hypomorphic Orc2 sumoylation (*orc2-K406R*) on the origin replication timing program, the $\log_2$ of the ratio between the *Z*-score determined for each origin in the relevant mutant to the *Z*-score for that origin in the wild-type *ORC2* strain was determined. Kernel density estimation was then used to generate a plot of $\log_2$ of the origin *Z*-score ratios versus density of replication origins. (*E*) The *orc2-K406R*/*ORC2* *Z*-score ratio for each origin was determined. The origins negatively affected (ratio cutoff of <0.8) or positively affected (ratio cutoff of >1.2) by *orc2-K406R* were then parsed by their experimentally determined Trep values, and the data are presented in histograms as in Figure 2C. The *P*-values for enrichment or depletion are as described in Figure 2C.

increased DNA lesions. Consistent with this finding, time-course experiments showed that *orc2-K406R* cells exhibited increased levels of checkpoint activation in late S/G2 phase, as evidenced by the increased phosphorylation of the checkpoint kinase Rad53, as well as increased levels of γH2A, an indicator for DNA lesions (Supplemental Fig. S7A). In addition, increased levels of Rad53 activation were also seen in *ORC2-SuON* cells compared with *ORC2-SuCtrl* (Supplemental Fig. S7B).

Another genetic indicator for the replication defect associated with both *ORC2-SuON* and *orc2-K406R* was slower growth upon the removal of the replication-promoting factor Rrm3, which is implicated in regulating both fork movement and ORC function (Syed et al. 2016). Both ORC alleles reduced the growth of *rrm3*Δ cells, while their corresponding controls did not (Fig. 7A,B; Supplemental Fig. S6A–C). Reduced cell growth of the *rrm3*Δ *ORC2-SuON* double mutant compared with either single mutant was clear from their smaller spore clone size, while the negative effect of *rrm3*Δ on *orc2-K406R* was more evident based on the cell-doubling time measurement (Fig. 7A; Supplemental Fig. S6C). These genetic data provided evidence that either ORC hypersumoylation or hyposumoylation enhanced the yeast's dependence on other important genome maintenance factors. Finally, rDNA stability was examined in cells containing *orc2-K406R* and those containing untagged or HA-tagged wild-type *ORC2*, as described above for *ORC2-SuON* (Fig. 4C). Similar to *ORC2-SuON*, *orc2-K406R* led to an increase in rDNA marker loss, providing evidence that ORC hyposumoylation affected genomic stability (Fig. 7C).

Discussion

Sumoylation regulates genome maintenance via targeting multiple substrates. While proteomic studies have established that yeast and human ORC subunits are sumoylated under stress conditions, the work here provided evidence that yeast Orc1, Orc2, Orc4, and Orc5 subunits are sumoylated during normal growth. We constructed two complementary ORC alleles resulting in hypersumoylated and hyposumoylated ORC to address the biological consequences of ORC sumoylation on genome replication and stability. High-resolution genome-scale analyses of chromosome replication revealed that ORC hypersumoylation and hyposumoylation had opposing

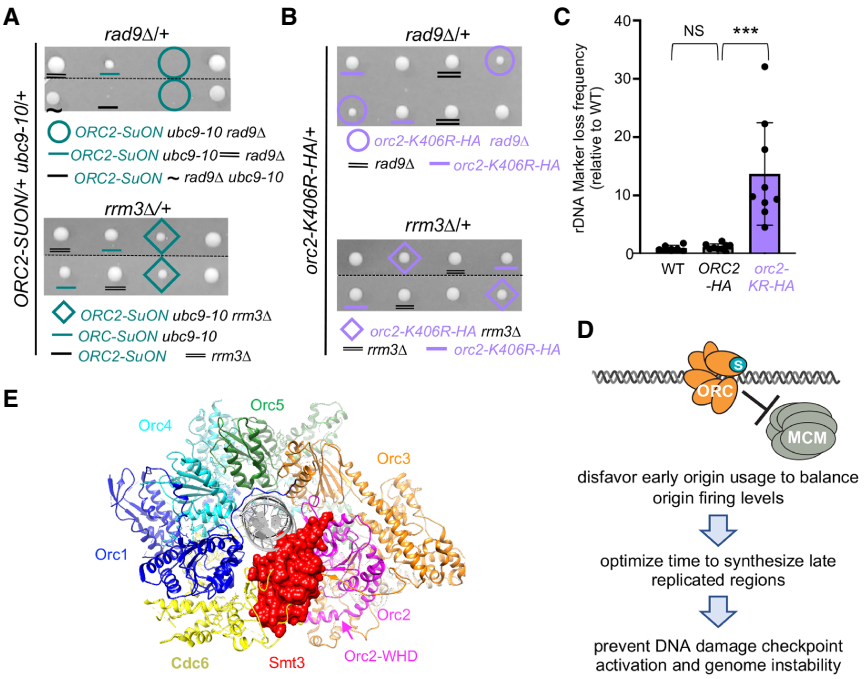

Figure 7. Genetic analysis of the ORC hyposumoylation or hypersumoylation alleles and a structural model for Orc2 sumoylation. (*A*,*B*) Genetic interactions between *ORC2-SuON* (*A*) and *orc2-K406R* (*B*) with *rad9*Δ or *rrm3*Δ. Controls for *ORC2-SuON* and *orc2-K406R* did not show negative interactions with either *rad9*Δ or *rrm3*Δ (Supplemental Fig. S6). Representative tetrads heterozygous of the indicated genotype are shown. Cells were grown for 3 d at 24°C in *A* and for 2 d at 30°C in *B*. (*C*) The effect of *orc2-K406R* on rDNA marker loss was determined as in Figure 4C. An unpaired two-tailed *t*-test was used to generate a *P*-value of <0.001 (***) for the difference between two types of cells. (*D*) A model for how ORC sumoylation affected replication initiation and genome stability was consistent with the data. ORC sumoylation disfavors MCM association at a subset of early origins. This regulation allowed for a more balanced distribution of licensed origins across chromosomes that promoted timely replication of genomic regions duplicating late in S phase. In the absence of this balance, checkpoint activation mechanisms were stimulated, and rDNA instability ensued. (*E*) A structural view of how Orc2 K406 sumoylation (SUMO, red) may sterically interfere with Orc2-WHD conformational changes that aid MCM recruitment and/or Cdc6 binding to ORC that is essential for MCM recruitment (Feng et al. 2021).

effects, with the former showing attenuating and the latter showing enhancing effects on subsets of early origins. These opposing phenotypic outcomes support the conclusion that sumoylation inhibited ORC activity. The role of ORC hypersumoylation was further assessed using biochemically reconstituted sumoylation and MCM loading systems, which revealed an inhibitory effect of ORC sumoylation on origin licensing. Taken together, our findings supported a model in which ORC sumoylation preferentially impairs the use of a subset of early origins via disfavoring MCM recruitment onto origins (Fig. 7D). Despite opposing effects on origin function, both hypersumoylated and hyposumoylated ORC reduced genome stability and increased the dependence on genome maintenance factors for growth. We thus propose that tipping the balance of ORC sumoylation status in one direction or the other influences the balance of origin function distributed across chromosomes and that ORC sumoylation status fine-tunes the level and distribution of origin licensing required for genome stability (Fig. 7D).

Biological consequences of ORC hypersumoylation and hyposumoylation

Alteration of substrate sumoylation status provides an effective strategy for assessing the functions of specific sumoylation. The *ORC2-SuON* allele enhanced sumoylation of Orc2 as well as Orc1 and Orc4, without changing global sumoylation levels or the sumoylation status of Mcm2 or Mcm3, which directly interacts with ORC. Although it is difficult to completely exclude off-target effects, these data provided evidence that *ORC2-SuON* limited up-regulation of sumoylation to ORC itself. Notably, *ORC2-SuON* led to yeast inviability, which was suppressed by a mild SUMO E2 mutant (*ubc9-10*) with concomitant reduction in Orc2 sumoylation. Thus, haploid *ORC2-SuON ubc9-10* cells could be used for experiments and compared with *ORC2-SuCtrl* in congenic *ubc9-10* backgrounds. Chromosomal replication analyses revealed that *ORC2-SuON* reduced the quantitative replication values of a subset of early origins. In addition, *ORC2-SuON* led to rDNA stability defects, consistent with reduced ORC activity. Thus, ORC hypersumoylation attenuates the essential role for ORC in origin function.

We also generated an ORC hyposumoylation mutant by focusing on Orc2. To achieve this feat, the sumoylation sites on endogenous Orc2 were identified using biochemical enrichment and mass spectrometry. While four sites were identified, systematic mutational analyses revealed that one (K406) was a major site for Orc2 sumoylation. K406 is conserved only within the *Saccharomyces* genus (Fig. 5B), and *orc2-K406R* exhibited normal Orc2 levels and Orc2 association with chromatin, as well as cell viability. However, *orc2-K406R* enhanced the firing of a subset of early origins, thus producing an origin phenotype that was generally the opposite of that produced by *ORC2-SuON*. These results provided additional support to the notion that ORC sumoylation inhibited early origin licensing and that its levels were tuned to optimize ORC functions for normal yeast growth.

We note that in the two examined ORC mutants, early and late origins were still fired early and late in S phase,

consistent with the theory that replication timing is controlled at the level of origin activation, not licensing. With this said, loaded MCM is the substrate for origin activation factors; thus, alterations in origin licensing efficiencies affect origins' competitiveness for activation factors. Our data suggest that ORC sumoylation status influences the relative replication probability of origins at the levels of origin licensing efficiency.

Proper ORC sumoylation status is required for genomic stability and cell fitness

While ORC hypersumoylation and hyposumoylation affected origin function in opposing directions, they both compromised genome stability and growth. Both types of alleles led to rDNA instability. In addition, even though *orc2-K406R* enhanced the firing of early origins and accelerated entry into S phase, the mutant cells were delayed in completing S phase compared with wild-type controls. Genetic data provided additional evidence that both ORC hypersumoylation and hyposumoylation compromised cell fitness, as these ORC states sensitized the growth of cells lacking two genome maintenance proteins, including the checkpoint protein Rad9 and the Rrm3 helicase that is implicated in regulating ORC and promoting replication fork progression through challenging chromosomal structures (Syed et al. 2016). The genetic interactions with *rrm3*Δ could reflect an enhanced requirement of Rrm3 when the origin firing program is altered. In the case of *orc2-K406R*, checkpoint activation and an increase in γH2A levels were detected in G2 phase, suggesting that genome lesions are generated. The simplest interpretation is that excessive activation of early origins due to *orc2-K406R* limited the ability of late regions to complete replication by the end of S phase, thus leaving DNA gaps that can induce the Rad9 checkpoint and produce genomic instability (Fig. 7D). Other possibilities cannot be excluded, such as those yet-to-be-defined genome maintenance defects caused by two opposing Orc2 alleles. For example, the enhanced origin licensing associated with Orc2 hyposumoylation might cause early origin refiring and partial DNA rereplication. In addition, given that stress conditions can alter both protein sumoylation and origin firing, ORC sumoylation may change origin licensing in response to some of these conditions to avoid replication fork transcription conflicts that might arise due to transcriptional changes in response to stress. Changes in origin licensing could also be used to help promote mutagenesis, which in turn could help cells adapt to new stressful environments.

ORC sumoylation acts to modulate the efficiency of origin licensing

ORC must perform multiple biochemical steps to load the double-hexameric MCM onto DNA (origin licensing) (Stillman 2022). Hypersumoylated ORC associated with DNA in vitro and hyposumoylated ORC did not reduce its chromatin association, suggesting that sumoylation does not significantly affect ORC association with DNA. In contrast, both in vivo and in vitro data suggest that hypersumoylated ORC impaired MCM recruitment to DNA. We note that higher in vitro ORC sumoylation levels compared with in vivo levels may lead to stronger effects on MCM loading than occur in vivo. Nevertheless, the consistency between the biochemical data and the in vivo data supported a model in which origin licensing efficiency is regulated by sumoylated ORC on origin DNA, with ORC sumoylated forms attenuating the efficiency of the MCM recruitment step (Fig. 7D). This mechanistic explanation was adequate to explain the genome-scale replication data generated for this report, but further experiments defining the dynamics of ORC sumoylation in vivo could inform us of the more precise role of this modification. For example, examining Orc2 sumoylation during the cell cycle showed that its level increased as cells progressed through S phase and decreased in G2–M phase (Supplemental Fig. S8). These data raise the possibility that Orc2 sumoylation might play a role in preventing relicensing of origins in late S phase, a hypothesis that will be examined in the future. In the meantime, additional examination of ORC sumoylation in vitro can inform us how sumoylated ORC impedes MCM recruitment in vitro, and this would benefit from careful titration experiments of ORC sumoylation to establish conditions that match in vivo ORC sumoylation. While a more complete understanding of the molecular roles of ORC sumoylation require further investigation, recent structural data offer potential insight. Specifically, in a recent cryo-EM structure of the ORC–Cdc6 complex, Orc2-K406 is located on the surface of the ORC complex proximal to both the Cdc6 binding site and Orc2-WHD (Feng et al. 2021). As SUMO is flexibly tethered to its modification site in other substrates (Powers et al. 2018; Attali et al. 2021), it is probable that sumoylation at this site can sterically impede one or more MCM recruitment steps (Fig. 7E). While this model can provide an explanation for the negative effects of ORC sumoylation on MCM loading, the current data cannot yet indicate the full set of sumoylation site(s) on ORC most relevant to its functional regulation.

Models for ORC sumoylation dynamics and future challenges

The sumoylated forms of most substrates represent only a small fraction of the total amount of corresponding proteins (Zhao 2018). This observation holds for replication initiation factors such as Dbf4 and Mcm2-7 subunits and for the ORC subunits described here (Wei and Zhao 2016; Psakhye et al. 2019). The small fraction of sumoylated proteins present at a given moment might be explained, at least in part, by the highly dynamic sumoylation and desumoylation cycles. However, it remains unclear how such a low level of sumoylation on a given protein (for this discussion, ORC) leads to a functional outcome. We considered three nonexclusive possibilities. First, sumoylation of ORC may occur efficiently only at specific loci. Perhaps different levels of desumoylation and/or sumoylation enzymes exist at different origins, such that only ORC at a subset of origins maintains a level

of sumoylation sufficient to inhibit origin licensing. Second, we considered a "SUMO flicker" model, in which cycles of sumoylation and desumoylation reduce the time windows for unmodified ORC to complete the multistep MCM loading reaction. Indeed, controlling the probability of a complete MCM loading reaction has been proposed as a mechanism for balancing the distribution of licensed origins across yeast chromosomes (Das et al. 2015; Hoggard et al. 2020). Third, a "collective effect" model suggests that sumoylation of any one of the six ORC subunits would be sufficient to attenuate origin licensing, with sumoylation on more subunits leading to stronger inhibition. This model could explain the stronger genetic interactions seen for Orc2-SuON than for *orc2-K406R* (Fig. 7A,B). Future investigations, including mapping additional sumoylated sites on ORC subunits, will be required to address these models.

While yeast and human origin control differ in many respects, it is notable that a small fraction of human Orc2 is sumoylated where it promotes recruitment of the KDM5A histone deacetylase, which in turn generates a heterochromatin state that prevents rereplication of centromeric DNA (Huang et al. 2016). Thus, despite the differences between yeast and human ORC regulation, as well as yeast and human origins, in both organisms, sumoylated Orc2 helps to restrain origin function.

Materials and methods

Yeast strains and procedures

Standard procedures were used for cell growth, medium preparation, epitope tagging at endogenous loci, and tetrad dissection, unless otherwise indicated. All strains are isogenic to W1588-4C, a *RAD5* derivative of W303 (*MATa ade2-1 can1-100 ura3-1 his3-11,15 leu2-3,112 trp1-1 rad5-535*) and are listed in Supplemental Table S1. Mutations were introduced using a standard one-step integration PCR-based method. Correct tagging and mutations were verified by sequencing. The SuON tag was comprised of amino acids 418–621 of the SUMO binding domain of Ulp1, with the C580S substitution to abolish enzymatic activity, while the SuCtrl tag contained one additional substitution that abolished the high-affinity SUMO binding site (F474A) (Lei and Zhao 2017). At least two biological isolates of the same genotype were examined for each experiment. Strains containing *ubc9-10* were examined at its permissive temperature of 24°C. Doubling time of yeast cells were measured as described (Hung et al. 2018). Briefly, cells were grown in a 96-well plate at 30°C with OD600 measured every 15 min for 24 h, and doubling times were calculated from these data using a custom R script.

Synchronization and FACS analyses

Standard methods were used to synchronize yeast cells in G1 phase using α factor (Dhingra et al. 2019). *ubc9-10* log-phase cells were treated for 3 h with three doses of 5 ug/mL α factor, each added at 1-h intervals. Wild-type *UBC9* log-phase cells were treated for 1 h with 5 ug/mL α factor followed by the addition of 2.5 ug/mL α factor for another 30 min. When 95% cells had reached G1 arrest based on the presence of unbudded cells, cells were washed and released into fresh media without α factor to allow for entry into S phase. For PFGE gel analyses, 15 ug/mL nocodazole was added 30 min after G1 release to prevent cells from exiting the first cell cycle. Cell cycle stages were confirmed by flow cytometry analyses (FACS) using standard procedures on a FACSCalibur flow cytometer, and data were analyzed with FCS7 software as described previously (Dhingra et al. 2019).

Detection of protein sumoylation by Ni-PD

Standard Ni-NTA pull-down was performed as previously described (Ulrich and Davies 2009). In brief, protein extracts prepared in 55% TCA were incubated in buffer A (6 M guanidine HCl, 100 mM sodium phosphate at pH 8.0, 10 mM Tris-HCl at pH 8.0) with rotation for 1 h at room temperature. The cleared supernatant was obtained after centrifugation for 20 min and was then incubated with Ni-NTA resin (Qiagen) in the presence of 0.05% Tween 20 and 4.4 mM imidazole overnight at room temperature with rotation. Beads were washed twice with buffer A supplemented with 0.05% Tween 20 and then four times with buffer C (8 M urea, 100 nM sodium phosphate at pH 6.3, 10 mM Tris-HCl at pH 6.3) supplemented with 0.05% Tween 20. HU buffer (8 M urea, 200 mM Tris-HCl at pH 6.8, 1 mM EDTA, 5% SDS, 0.1% bromophenol blue, 1.5% DTT, 200 mM imidazole) was used to elute proteins from the beads. Samples were loaded onto a 4%–12% gradient Tris-glycine gel (Bio-Rad). Western blotting probed with antibodies recognizing the tagged proteins detected both sumoylated and unmodified substrates. The unmodified forms of the substrates were detected due to nonspecific binding to the Ni-NTA beads and were not enriched in samples from cells expressing 8His-tagged yeast SUMO (Smt3). Denaturing conditions during protein extraction minimized desumoylation.

Enrichment of endogenously sumoylated Orc2 for mass spectrometry

Eight liters of cell cultures from strains containing 8His-Smt3 and Orc2-HA was harvested. Note that in order to facilitate SUMO (Smt3) identification in mass spectrometry, the most C-terminal Ile of Smt3 was replaced by Arg to enable trypsin cleavage at this site. This variant of Smt3 (I96R) has been shown to support normal SUMOylation function (Albuquerque et al. 2015). Cells were frozen in droplets with liquid nitrogen and then ground into powder in a freezer mill (Freezer/Mill 6875D). The powder was thawed on ice, and cell extracts were brought to a final concentration of 14% TCA and pelleted by centrifugation. After removing TCA, the pellets were washed with acetone and then resolubilized in buffer A as described above with shaking at 30°C. Cleared supernatant supplemented with 0.05% Tween 20 and 4.4 mM imidazole was then incubated with Ni-NTA resin (Qiagen) overnight at room temperature. Beads were washed once with buffer A containing 0.05% Tween 20 and once with buffer C as described above with 0.05% Tween 20. HU buffer described above was used to elute proteins from the beads. Eluted protein was then dialyzed for 2 h at room temperature against the RIPA buffer (150 mM NaCl, 50 mM Tris at pH7.4, 5 mM EDTA, 1.25% Triton X-100, 10 mM N-ethylmelamide). Protein extract was then incubated with agarose beads cross-linked to HA antibodies and rotated overnight at 4°C. Beads were washed once with RIPA buffer and with triethylammonium bicarbonate (TEAB) buffer (Sigma) before elution with 5% SDS in TEAB. Samples loaded onto a 4%–12% gradient Tris-glycine gel (BioRad) were examined by immunoblotting with anti-HA antibody and confirmed the presence of Orc2 sumoylated forms prior to mass spectrometry.

Immunoblotting analysis and antibodies

Protein samples were examined by SDS-PAGE and transferred to a 0.2-μm nitrocellulose membrane (GE G5678144) for

immunoblotting. Antibodies used were anti-HA (3F10), anti-V5 (Invitrogen R960-25), PAP (Sigma P1291), anti-Rad53 (Santa Cruz Biotechnology yC-19), anti-Pgk1 (Invitrogen 22C5D8), anti-Orc1 (3E9) (Gabrielse et al. 2006), anti-Orc4 (1B1) (Gabrielse et al. 2006), and anti-Smt3 (Zhao and Blobel 2005). Validation of antibodies was provided either on the manufacturers' websites or in the cited references. For quantification purposes, membranes were scanned with a Fujifilm LAS-3000 luminescent image analyzer, which had a linear dynamic range of 10^4. Quantification of blots and generation of figures were performed with ImageJ and Photoshop.

Trichloroacetic acid (TCA) protein extraction

To examine protein levels and Rad53 phosphorylation, cell extracts were prepared as reported (Dhingra et al. 2019). Cell pellets were resuspended in 20% TCA and lysed by glass bead beating. The lysate was centrifuged to remove supernatant. Precipitated proteins were resuspended in Laemmli buffer (65 mM Tris-HCl at pH 6.8, 2% SDS, 5% 2-mercaptoethanol, 10% glycerol, 0.025% bromophenol blue) with 2 M Tris to neutralize the solution. Prior to loading, samples were boiled for 5 min and spun down at 12,000 rpm for 10 min to remove insoluble materials.

Chromatin fractionation

Chromatin fractionation was performed as described previously with minor modifications (Schepers and Diffley 2001). Spheroplasts were lysed in lysis buffer containing 1% Triton X-100 and were laid on a 30% sucrose cushion and centrifuged at 13,000 rpm for 20 min to separate the supernatant and chromatin fractions. The chromatin-bound fraction was washed with lysis buffer and resuspended in the same buffer. Equal volumes of samples from lysate, supernatant, and chromatin fractions were precipitated with 20% TCA and resuspended in Laemmli buffer with the addition of 2 M Tris to neutralize TCA.

Pulsed-field gel electrophoresis (PFGE)

PFGE was performed as previously described (Cremona et al. 2012). Cells were addressed in G1 phase and then released into the cell cycle. Cells harvested from the indicated time points in Figure 4A were embedded in agarose plugs, spheroplasted, and deproteinized. Plugs were loaded into 0.5× TBE gels and run on a CHEF-DR III pulsed-field electrophoresis system (Bio-Rad) for 12 h to achieve chromosome separation. Gels were stained by ethidium bromide. Chromosome signal was measured using ImageJ and normalized to the G1 signal. The position of each chromosome was derived as described in Lai (1993).

rDNA marker loss frequency

The loss frequency of the *ADE2-CAN1* cassette inside the rDNA array was measured as previously described (Fritze et al. 1997). Cells were grown to stationary phase over equal doubling times and plated on synthetic complete (SC) media for cell count totals. Cells were additionally plated on media containing canavanine (SC + Can) and incubated for 2 d at 30°C, after which colonies were counted. The frequency of marker loss was calculated as previously described using the formula $F_R = N_{can}/N_C$, where N_{Can} is the number of colonies on SC + Can plates and N_C is the number of cells plated on SC plates (Bernstein et al. 2011).

Whole-genome sequencing and copy number calculation

G1-arrested cells were released into cell cycle at 24°C, and S-phase progression was monitored by FACS. For *ORC2-SuON ubc9-10* and *ORC2-SuCtrl ubc9-10* cells growing at 24°C, S-phase samples were collected 40 min after G1, whereas 30-min samples after G1 release were examined for *ORC2-HA* and *orc2-K406R-HA* cells growing at 30°C. For both G1- and S-phase samples, 1.5 µg of genomic DNA was used to generate libraries using a KAPA library kit at the iGO facility (Memorial Sloan Kettering Cancer Center [MSKCC]) and sequenced with a HiSeq 4000 (Illumina and MSKCC) or a NextSeq1000 (Illumina) in the Department of Biomolecular Chemistry of the University of Wisconsin at Madison. At least 10 million 50-bp paired-end reads were generated per sample. Copy number calculation and chromosome map were derived following the general procedure as reported (Batrakou et al. 2020). In brief, reads were first mapped to the S288c reference genome (SGD; SacCer3), excluding repetitive sequences, and then summed in 0.5-kb bins with Genome Browser. Bins containing <600 reads were excluded. For each strain, the binned reads from S-phase samples at a given locus were divided by those from the G1 sample and normalized to the ratio of total reads. The normalized S/G1 read ratio was then adjusted to be between 1 and 2 based on the percentage of replication of the sample to derive a relative copy number of the particular locus. The maps of adjusted copy numbers were smoothed with the LOESS function. The sequencing data were deposited in the SRA database. The data sets were assigned the Biosample accession number PRJNA821839

Z-score analysis

Z-scores were calculated as described in Hoggard et al. (2021). Briefly, sequencing coverages for each genomic nucleotide within *ORC2-SuON*, *ORC2-SuCtrl*, *orc2-KR-HA*, and *ORC2-HA* S phase were determined. The G1 sample was normalized for sequencing depth and breadth (Skene and Henikoff 2015) and then mapped to 1015 windows, as defined in Hoggard et al. (2021), containing both origin and nonorigin loci and spanning 10,001 bp (ORC site start ± 5 kb). Thus mapped, coverages within each window were summed and then converted to S/G1 ratios. *Z*-scores for each window within a particular strain were calculated using the following equation: $Z\text{-score} = (S/G1_{ratio} - \mu)/\sigma$, where µ and σ are the mean and standard deviation of all S/G1 ratios in a population, respectively. Only windows associated with confirmed origins are shown in the figures. Confirmed origins were placed in three cohorts based on the Trep value measured in Yabuki et al. (2002). Origins with the lowest one-third of Trep values, consistent with the earliest replicating origins, were considered early, origins with the highest one-third of Trep values, consistent with latest replicating origins, were considered late. Origins with values between the two were considered midfiring.

Mass spectrometry and data analysis

Samples enriched for sumoylated Orc2 were reduced in 4 mM TCEP (Pierce), alkylated by 10 mM iodoacetamide (Sigma), and then quenched using 10 mM DTT (Fisher) with 30-min reaction time at each step at room temperature in the dark. The resulting sample was then loaded onto S traps (Protifi) according to the manufacturer's instructions and then digested overnight at 37°C with trypsin (Promega). Digested peptides were eluted from the S trap and lyophilized for 48 h. Lyophilized peptides were resuspended in 0.1% trifluoroacetic acid (TFA; Fisher) and fractionated with high-pH reversed-phase chromatography (Pierce). Fractionated peptides were lyophilized and resuspended in 0.1%

TFA. Peptide concentrations of the fractions were estimated with fluorometric quantitative peptide assay (Pierce). From each fraction, 250 ng of peptides was loaded onto a Bruker nano-elute UPLC in line with a Bruker TIMS-TOF Pro mass spectrometer and eluted with a 45-min acetonitrile gradient. Raw TOF data were searched with PEAKS Studio X+ (Bioinformatic Solutions, Inc.) against a yeast proteome downloaded from UniProt (http://www.uniprot.org), with precursor and fragment mass accuracy at 10 ppm, two missed cleavages, carbamidomethyl cysteine as fixed modification, methionine oxidation, peptide N-terminal acetylation, and diglycylyl lysine (GlyGly) as variable modifications, and five modifications allowed per peptide. Identified sites were verified by manual inspection of MS2 spectra. The mass spectrometry proteomics data have been deposited to the ProteomeXchange Consortium (Deutsch et al. 2020) via the PRIDE (Perez-Riverol et al. 2022) partner repository with the data set identifier PXD032977.

Structure model

The structure of the yeast ORC bound to Cdc6 and origin DNA (PDB: 7mca) as described in Feng et al. (2021) was analyzed in the Chimera software (Pettersen et al. 2004) with the addition of yeast SUMO (PDB: 2EKE) as described by Duda et al. (2007). One orientation of the SUMO is depicted in Figure 7E to highlight its potential to interfere with Cdc6 binding to ORC and/or the conformational change of the Orc2 WHD.

Protein purification

ORC, Cdc6, and Cdt1·Mcm2-7 were purified as previously described (Gros et al. 2015). SUMO, SUMO E1, SUMO E2, and the Siz1 and Siz2 SUMO E3s were purified as described (Zhao and Blobel 2005). Ulp1 was expressed in *E. coli* strain BL21 DE3 codon + RIL. Cells were grown at 37°C to each 0.7 OD600 in LB supplemented with 50 mg/mL kanamycin and 34 mg/mL chloramphenicol, followed by cooling for 10 min in an ice bath. Induction was carried out for 4 h at 30°C by the addition of 1 mM IPTG. Cells were harvested, resuspended in lysis buffer (50 mM Tris-HCl at pH 8.0, 300 mM NaCl, 0.05% NP-40, 10% glycerol, 2 mM 2-mercaptoethanol) supplemented with protease inhibitor cocktail, and lysed by sonication. Extracts were centrifuged at 15,000 rpm for 20 min in an SS34 rotor. The resulting soluble phase was recovered, supplemented with 10 mM imidazole, and passed over a 5-mL His-trap column. The resin was washed with 10 column volumes of lysis buffer supplemented with 30 mM imidazole, and bound proteins were then eluted with a gradient of 30–400 mM imidazole in lysis buffer over 10 column volumes.

ORC sumoylation and MCM loading assays

A linear 1-kb DNA fragment containing ARS305 was generated by PCR and bound to streptavidin-coated M-280 Dynabeads as described (Remus et al. 2009). One picomole of DNA beads (25 nM) was incubated with 82.5 nM ORC. ORC sumoylation reactions were performed in 40 µL of reaction buffer [25 mM HEPES-KOH at pH 7.6, 0.1 M K-acetate, 0.02% NP-40, 10 mM $Mg(OAc)_2$, 5% glycerol, 1 mM DTT, 5 mM ATP] containing 25 nM SUMO E1 (Uba2-Aos1), 240 nM SUMO E2 (Ubc9), 170 nM SUMO E3s (Siz1 and Siz2), and 3.5 µM Smt3 that contained three lysine mutations to reduce SUMO chain formation. Reactions were mixed on ice and incubated using a thermoshaker (Eppendorf) under constant agitation at 1200 rpm for 30 min at 30°C. Beads were then washed once with 0.4 mL of low-salt wash buffer [25 mM HEPES-KOH at pH 7.6, 0.3 M K-acetate, 0.02% NP-40, 5 mM $Mg(OAc)_2$, 1 mM EDTA, 1 mM EGTA, 10% glycerol, 1 mM DTT] before being resuspended in 40 µL of fresh reaction buffer supplemented with or without 0.9 µM Ulp1 and incubated again at 1200 rpm for 30 min at 30°C. The reaction was once again washed with 0.4 mL of low-salt wash buffer before being resuspended in 40 µL of fresh reaction buffer supplemented with 85 nM Cdc6 and 275 nM Cdt1·Mcm2-7 and 5 mM either ATP or ATPγS. The reactions were again incubated at 1200 rpm for 30 min at 30°C. Beads were then washed once with 0.4 mL of low-salt wash buffer [25 mM HEPES-KOH at pH 7.6, 0.3 M K-acetate, 0.02% NP-40, 5 mM $Mg(OAc)_2$, 1 mM EDTA, 1 mM EGTA, 10% glycerol, 1 mM DTT] and once with 0.4 mL of either low-salt buffer or high-salt wash buffer (as low-salt buffer, but 0.5 M NaCl instead of 0.3 M K-acetate). The beads were finally resuspended in 1× Laemmli buffer (2% SDS, 60 mM Tris-Cl at pH 6.8, 5% 2-mercaptoethanol, 0.003% [w/v] bromophenol blue, 10% glycerol) before being analyzed by either Western blot or silver-stained SDS-PAGE.

Competing interest statement

The authors declare no competing interests.

Acknowledgments

We thank the Zhao laboratory members for discussions, Dr. Meng-Qiu Dong at the National Institute of Biological Sciences for initial help with mass spectrometry, and Dr. Yuangliang Zhai at the University of Hong Kong for help with structural modeling. This work was supported by National Institutes of Health (NIH) R01GM131058 and R35 GM145260 to X.Z., NIH R35GM141641 to C.A.F., NIH R01-GM107239 to D.R., and NIH GM074223 to N.H. N.H. is an investigator with the Howard Hughes Medical Institute.

Author contributions: G.R.-M., G.L., D.R., N.H., and X.Z. designed the experiments. G.R.-M. performed in vivo experiments. G.L. performed in vitro tests. T.H. and G.R.-M. performed analysis of the whole-genome sequencing experiments. N.B. and G.R.-M. performed mass spectrometry experiments and data analysis. G.R.-M. and X.Z. wrote the manuscript with editing from D.R. and C.A.F.

References

Albuquerque CP, Yeung E, Ma S, Fu T, Corbett KD, Zhou H. 2015. A chemical and enzymatic approach to study site-specific sumoylation. *PLoS One* **10:** e0143810. doi:10.1371/journal.pone.0143810

Almedawar S, Colomina N, Bermúdez-López M, Pociño-Merino I, Torres-Rosell J. 2012. A SUMO-dependent step during establishment of sister chromatid cohesion. *Curr Biol* **22:** 1576–1581. doi:10.1016/j.cub.2012.06.046

Attali I, Botchan MR, Berger JM. 2021. Structural mechanisms for replicating DNA in eukaryotes. *Annu Rev Biochem* **90:** 77–106. doi:10.1146/annurev-biochem-090120-125407

Batrakou DG, Müller CA, Wilson RHC, Nieduszynski CA. 2020. DNA copy-number measurement of genome replication dynamics by high-throughput sequencing: the sort-seq, sync-seq and MFA-seq family. *Nat Protoc* **15:** 1255–1284. doi:10.1038/s41596-019-0287-7

Bell SP, Labib K. 2016. Chromosome duplication in *Saccharomyces cerevisiae*. *Genetics* **203:** 1027–1067. doi:10.1534/genetics.115.186452

Bell SP, Stillman B. 1992. ATP-dependent recognition of eukaryotic origins of DNA replication by a multiprotein complex. *Nature* **357:** 128–134. doi:10.1038/357128a0

Bernstein KA, Reid RJ, Sunjevaric I, Demuth K, Burgess RC, Rothstein R. 2011. The Shu complex, which contains Rad51 paralogues, promotes DNA repair through inhibition of the Srs2 anti-recombinase. *Mol Biol Cell* **22:** 1599–1607. doi:10.1091/mbc.E10-08-0691

Bonner JN, Choi K, Xue X, Torres NP, Szakal B, Wei L, Wan B, Arter M, Matos J, Sung P, et al. 2016. Smc5/6 mediated sumoylation of the Sgs1–Top3–Rmi1 complex promotes removal of recombination intermediates. *Cell Rep* **16:** 368–378. doi:10.1016/j.celrep.2016.06.015

Cremona CA, Sarangi P, Yang Y, Hang LE, Rahman S, Zhao X. 2012. Extensive DNA damage-induced sumoylation contributes to replication and repair and acts in addition to the Mec1 checkpoint. *Mol Cell* **45:** 422–432. doi:10.1016/j.molcel.2011.11.028

Das SP, Borrman T, Liu VW, Yang SC, Bechhoefer J, Rhind N. 2015. Replication timing is regulated by the number of MCMs loaded at origins. *Genome Res* **25:** 1886–1892. doi:10.1101/gr.195305.115

Debatisse M, Le Tallec B, Letessier A, Dutrillaux B, Brison O. 2012. Common fragile sites: mechanisms of instability revisited. *Trends Genet* **28:** 22–32. doi:10.1016/j.tig.2011.10.003

Deutsch EW, Bandeira N, Sharma V, Perez-Riverol Y, Carver JJ, Kundu DJ, Garcia-Seisdedos D, Jarnuczak AF, Hewapathirana S, Pullman BS, et al. 2020. The ProteomeXchange consortium in 2020: enabling 'big data' approaches in proteomics. *Nucleic Acids Res* **48:** D1145–D1152. doi:10.1093/nar/gkz984

Dhingra N, Wei L, Zhao X. 2019. Replication protein A (RPA) sumoylation positively influences the DNA damage checkpoint response in yeast. *J Biol Chem* **294:** 2690–2699. doi:10.1074/jbc.RA118.006006

Duda DM, van Waardenburg RC, Borg LA, McGarity S, Nourse A, Waddell MB, Bjornsti MA, Schulman BA. 2007. Structure of a SUMO-binding-motif mimic bound to Smt3p-Ubc9p: conservation of a non-covalent ubiquitin-like protein–E2 complex as a platform for selective interactions within a SUMO pathway. *J Mol Biol* **369:** 619–630. doi:10.1016/j.jmb.2007.04.007

Fang D, Lengronne A, Shi D, Forey R, Skrzypczak M, Ginalski K, Yan C, Wang X, Cao Q, Pasero P, et al. 2017. Dbf4 recruitment by forkhead transcription factors defines an upstream rate-limiting step in determining origin firing timing. *Genes Dev* **31:** 2405–2415. doi:10.1101/gad.306571.117

Feng X, Noguchi Y, Barbon M, Stillman B, Speck C, Li H. 2021. The structure of ORC–Cdc6 on an origin DNA reveals the mechanism of ORC activation by the replication initiator Cdc6. *Nat Commun* **12:** 3883. doi:10.1038/s41467-021-24199-1

Fritze CE, Verschueren K, Strich R, Easton Esposito R. 1997. Direct evidence for SIR2 modulation of chromatin structure in yeast rDNA. *EMBO J* **16:** 6495–6509. doi:10.1093/emboj/16.21.6495

Gabrielse C, Miller CT, McConnell KH, DeWard A, Fox CA, Weinreich M. 2006. A Dbf4p BRCA1 C-terminal-like domain required for the response to replication fork arrest in budding yeast. *Genetics* **173:** 541–555. doi:10.1534/genetics.106.057521

Golebiowski F, Matic I, Tatham MH, Cole C, Yin Y, Nakamura A, Cox J, Barton GJ, Mann M, Hay RT. 2009. System-wide changes to SUMO modifications in response to heat shock. *Sci Signal* **2:** ra24. doi:10.1126/scisignal.2000282

Gros J, Kumar C, Lynch G, Yadav T, Whitehouse I, Remus D. 2015. Post-licensing specification of eukaryotic replication origins by facilitated Mcm2-7 sliding along DNA. *Mol Cell* **60:** 797–807. doi:10.1016/j.molcel.2015.10.022

Hawkins M, Retkute R, Müller CA, Saner N, Tanaka TU, de Moura AP, Nieduszynski CA. 2013. High-resolution replication profiles define the stochastic nature of genome replication initiation and termination. *Cell Rep* **5:** 1132–1141. doi:10.1016/j.celrep.2013.10.014

Hiraga S, Alvino GM, Chang F, Lian HY, Sridhar A, Kubota T, Brewer BJ, Weinreich M, Raghuraman MK, Donaldson AD. 2014. Rif1 controls DNA replication by directing protein phosphatase 1 to reverse Cdc7-mediated phosphorylation of the MCM complex. *Genes Dev* **28:** 372–383. doi:10.1101/gad.231258.113

Hoggard TA, Chang F, Perry KR, Subramanian S, Kenworthy J, Chueng J, Shor E, Hyland EM, Boeke JD, Weinreich M, et al. 2018. Yeast heterochromatin regulators Sir2 and Sir3 act directly at euchromatic DNA replication origins. *PloS Genet* **14:** e1007418. doi:10.1371/journal.pgen.1007418

Hoggard T, Müller CA, Nieduszynski CA, Weinreich M, Fox CA. 2020. Sir2 mitigates an intrinsic imbalance in origin licensing efficiency between early- and late-replicating euchromatin. *Proc Natl Acad Sci* **117:** 14314–14321. doi:10.1073/pnas.2004664117

Hoggard T, Hollatz AJ, Cherney RE, Seman MR, Fox CA. 2021. The Fkh1 Forkhead associated domain promotes ORC binding to a subset of DNA replication origins in budding yeast. *Nucleic Acids Res* **49:** 10207–10220. doi:10.1093/nar/gkab450

Huang C, Cheng J, Bawa-Khalfe T, Yao X, Chin YE, Yeh ETH. 2016. SUMOylated ORC2 recruits a histone demethylase to regulate centromeric histone modification and genomic stability. *Cell Rep* **15:** 147–157. doi:10.1016/j.celrep.2016.02.091

Hung CW, Martínez-Márquez JY, Javed FT, Duncan MC. 2018. A simple and inexpensive quantitative technique for determining chemical sensitivity in *Saccharomyces cerevisiae*. *Sci Rep* **8:** 11919. doi:10.1038/s41598-018-30305-z

Knott SR, Peace JM, Ostrow AZ, Gan Y, Rex AE, Viggiani CJ, Tavaré S, Aparicio OM. 2012. Forkhead transcription factors establish origin timing and long-range clustering in *S. cerevisiae*. *Cell* **148:** 99–111. doi:10.1016/j.cell.2011.12.012

Kwan EX, Foss EJ, Tsuchiyama S, Alvino GM, Kruglyak L, Kaeberlein M, Raghuraman MK, Brewer BJ, Kennedy BK, Bedalov A. 2013. A natural polymorphism in rDNA replication origins links origin activation with calorie restriction and lifespan. *PLoS Genet* **9:** e1003329. doi:10.1371/journal.pgen.1003329

Lai B. 1993. *Pulsed field gel electrophoresis: a practical guide*. Academic Press, San Diego, CA.

Lei W, Zhao X. 2017. Roles of SUMO in replication initiation, progression, and termination. *Adv Exp Med Biol* **1042:** 371–393. doi:10.1007/978-981-10-6955-0_17

Lei M, Kawasaki Y, Young MR, Kihara M, Sugino A, Tye BK. 1997. Mcm2 is a target of regulation by Cdc7–Dbf4 during the initiation of DNA synthesis. *Genes Dev* **11:** 3365–3374. doi:10.1101/gad.11.24.3365

Mantiero D, Mackenzie A, Donaldson A, Zegerman P. 2011. Limiting replication initiation factors execute the temporal programme of origin firing in budding yeast. *EMBO J* **30:** 4805–4814. doi:10.1038/emboj.2011.404

Papouli E, Chen SH, Davies AA, Huttner D, Krejci L, Sung P, Ulrich HD. 2005. Crosstalk between SUMO and ubiquitin

on PCNA is mediated by recruitment of the helicase Srs2p. *Mol Cell* **19:** 123–133. doi:10.1016/j.molcel.2005.06.001

Perez-Riverol Y, Bai J, Bandla C, García-Seisdedos D, Hewapathirana S, Kamatchinathan S, Kundu DJ, Prakash A, Frericks-Zipper A, Eisenacher M, et al. 2022. The PRIDE database resources in 2022: a hub for mass spectrometry-based proteomics evidences. *Nucleic Acids Res* **50:** D543–D552. doi:10.1093/nar/gkab1038

Pettersen EF, Goddard TD, Huang CC, Couch GS, Greenblatt DM, Meng EC, Ferrin TE. 2004. UCSF chimera—a visualization system for exploratory research and analysis. *J Comput Chem* **25:** 1605–1612. doi:10.1002/jcc.20084

Powers KT, Lavering ED, Washington MT. 2018. Conformational flexibility of ubiquitin-modified and SUMO-modified PCNA shown by full-ensemble hybrid methods. *J Mol Biol* **430:** 5294–5303. doi:10.1016/j.jmb.2018.10.017

Pozo PN, Matson JP, Cole Y, Kedziora KM, Grant GD, Temple B, Cook JG. 2018. Cdt1 variants reveal unanticipated aspects of interactions with cyclin/CDK and MCM important for normal genome replication. *Mol Biol Cell* **29:** 2989–3002. doi:10.1091/mbc.E18-04-0242

Psakhye I, Castellucci F, Branzei D. 2019. SUMO-chain-regulated proteasomal degradation timing exemplified in DNA replication initiation. *Mol Cell* **76:** 632–645.e6. doi:10.1016/j.molcel.2019.08.003

Remus D, Beuron F, Tolun G, Griffith JD, Morris EP, Diffley JF. 2009. Concerted loading of Mcm2-7 double hexamers around DNA during DNA replication origin licensing. *Cell* **139:** 719–730. doi:10.1016/j.cell.2009.10.015

Ryba T, Hiratani I, Sasaki T, Battaglia D, Kulik M, Zhang J, Dalton S, Gilbert DM. 2011. Replication timing: a fingerprint for cell identity and pluripotency. *PLoS Comput Biol* **7:** e1002225. doi:10.1371/journal.pcbi.1002225

Salim D, Bradford WD, Freeland A, Cady G, Wang J, Pruitt SC, Gerton JL. 2017. DNA replication stress restricts ribosomal DNA copy number. *PloS Genet* **13:** e1007006. doi:10.1371/journal.pgen.1007006

Sanchez JC, Kwan EX, Pohl TJ, Amemiya HM, Raghuraman MK, Brewer BJ. 2017. Defective replication initiation results in locus specific chromosome breakage and a ribosomal RNA deficiency in yeast. *PloS Genet* **13:** e1007041. doi:10.1371/journal.pgen.1007041

Saner N, Karschau J, Natsume T, Gierliński M, Retkute R, Hawkins M, Nieduszynski CA, Blow JJ, de Moura AP, Tanaka TU. 2013. Stochastic association of neighboring replicons creates replication factories in budding yeast. *J Cell Biol* **202:** 1001–1012. doi:10.1083/jcb.201306143

Schepers A, Diffley JF. 2001. Mutational analysis of conserved sequence motifs in the budding yeast Cdc6 protein. *J Mol Biol* **308:** 597–608. doi:10.1006/jmbi.2001.4637

Skene PJ, Henikoff S. 2015. A simple method for generating high-resolution maps of genome-wide protein binding. *Elife* **4:** e09225. doi:10.7554/eLife.09225

Smith L, Plug A, Thayer M. 2001. Delayed replication timing leads to delayed mitotic chromosome condensation and chromosomal instability of chromosome translocations. *Proc Natl Acad Sci* **98:** 13300–13305. doi:10.1073/pnas.241355098

Stillman B. 2022. The remarkable gymnastics of ORC. *Elife* **11:** e76475. doi:10.7554/eLife.76475

Sun J, Evrin C, Samel SA, Fernández-Cid A, Riera A, Kawakami H, Stillman B, Speck C, Li H. 2013. Cryo-EM structure of a helicase loading intermediate containing ORC–Cdc6–Cdt1–MCM2-7 bound to DNA. *Nat Struct Mol Biol* **20:** 944–951. doi:10.1038/nsmb.2629

Syed S, Desler C, Rasmussen LJ, Schmidt KH. 2016. A novel Rrm3 function in restricting DNA replication via an Orc5-binding domain is genetically separable from Rrm3 function as an ATPase/helicase in facilitating fork progression. *PLoS Genet* **12:** e1006451. doi:10.1371/journal.pgen.1006451

Tanaka S, Araki H. 2013. Helicase activation and establishment of replication forks at chromosomal origins of replication. *Cold Spring Harb Perspect Biol* **5:** a010371. doi:10.1101/cshperspect.a010371

Tanaka S, Nakato R, Katou Y, Shirahige K, Araki H. 2011. Origin association of Sld3, Sld7, and Cdc45 proteins is a key step for determination of origin-firing timing. *Curr Biol* **21:** 2055–2063. doi:10.1016/j.cub.2011.11.038

Ulrich HD, Davies AA. 2009. In vivo detection and characterization of sumoylation targets in *Saccharomyces cerevisiae*. *Methods Mol Biol* **497:** 81–103. doi:10.1007/978-1-59745-566-4_6

Watanabe Y, Maekawa M. 2010. Spatiotemporal regulation of DNA replication in the human genome and its association with genomic instability and disease. *Curr Med Chem* **17:** 222–233. doi:10.2174/092986710790149756

Wei L, Zhao X. 2016. A new MCM modification cycle regulates DNA replication initiation. *Nat Struct and Mol Bio* **23:** 209–216. doi:10.1038/nsmb.3173

Yabuki N, Terashima H, Kitada K. 2002. Mapping of early firing origins on a replication profile of budding yeast. *Genes Cells* **7:** 781–789. doi:10.1046/j.1365-2443.2002.00559.x

Zhao X. 2018. SUMO-mediated regulation of nuclear functions and signaling processes. *Mol Cell* **71:** 409–418. doi:10.1016/j.molcel.2018.07.027

Zhao X, Blobel G. 2005. A SUMO ligase is part of a nuclear multiprotein complex that affects DNA repair and chromosomal organization. *Proc Natl Acad Sci* **102:** 4777–4782. doi:10.1073/pnas.0500537102